Supporting Information

Acoustofluidic lysis of cancer cells and Raman spectrum profiling

Hyeono Nam[a], Jong-Eun Park[b], Waqas Waheed[c], Anas Alazzam[c], Hyung Jin Sung[a,*], and Jessie S. Jeon[a*]

[a]*Department of Mechanical Engineering, Korea Advanced Institute of Science and Technology, Daejeon 34141, Republic of Korea*
[b]*Department of Mechanical Engineering, The State University of New York Korea, Incheon 21985, Republic of Korea*
[c]*Department of Mechanical Engineering, Khalifa University, Abu Dhabi, UAE*
*Corresponding authors

Supporting information includes:

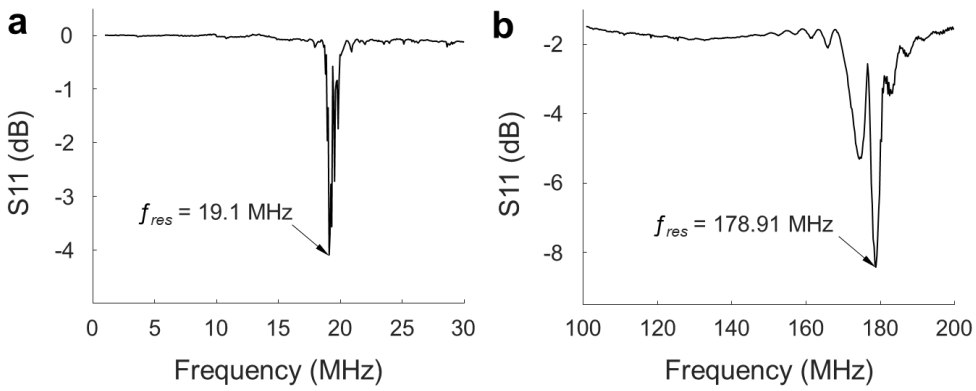

Figure S1. Scattering parameters for each frequency. a) Nominal frequency of 20 MHz denotes a resonance frequency of 19.1 MHz. b) Nominal frequency of 180 MHz denotes a resonance frequency of 178.91 MHz.

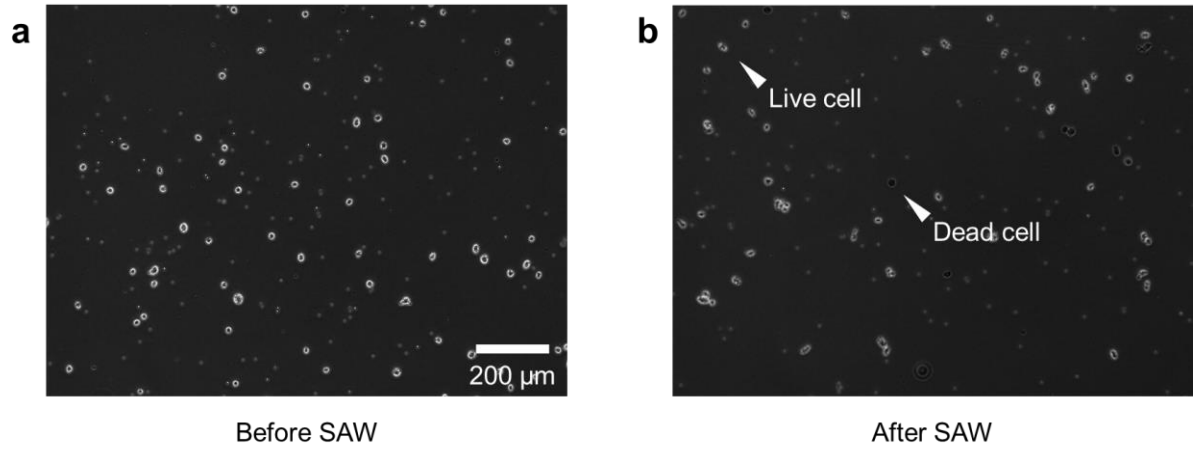

Figure S2. Bright field image of 0.4 % Trypan blue-stained cells. a) before and b) after SAW at 19.1 MHz for 3 minutes with 4×10^6 particles per mL of PSMPs and 1×10^6 cells per mL of MDA-MB-231.

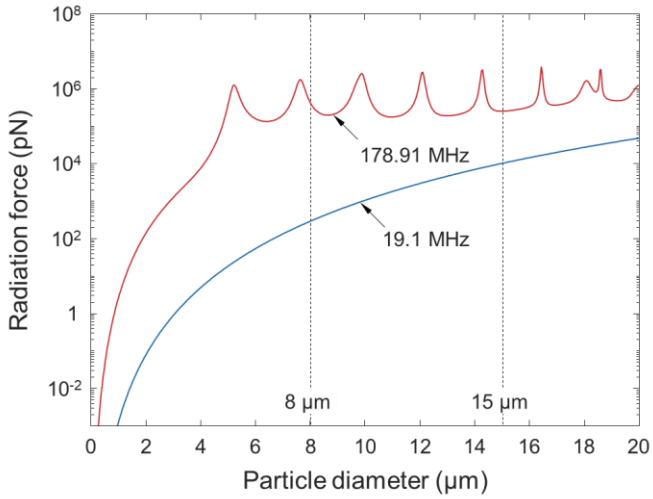

Figure S3. Theoretical ARF for each frequency with respect to PSMP diameter.

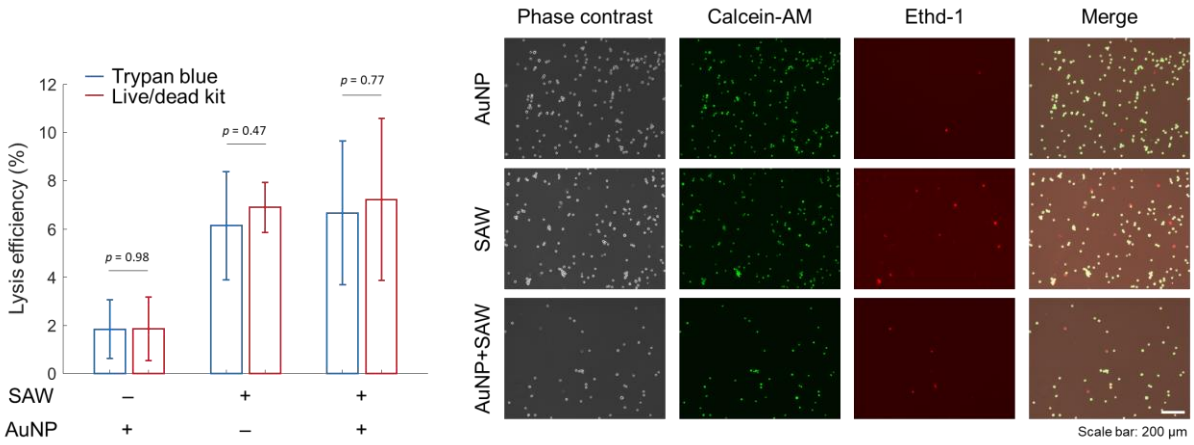

Figure S4. SAW-induced cell lysis with AuNPs. Lysis efficiencies under 178.91 MHz with or without AuNP denote relatively insufficient momentum of AuNPs. (n = 6, three technical repeats from two independent experiments, error bars represent standard deviation, p-value means not significant via unpaired student's t-test).

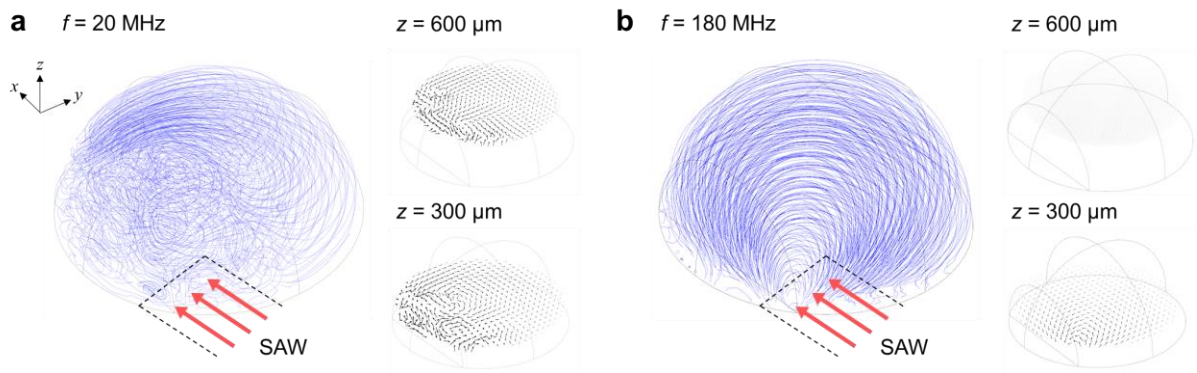

Figure S5. Computational results of SAW-induced streamlines and velocity vectors in a sessile droplet. Visualization of overall streamlines and velocity vectors in the horizontal planes (z = 300 μm and 600 μm) at a frequency of a) 20 MHz, and b) 180 MHz.

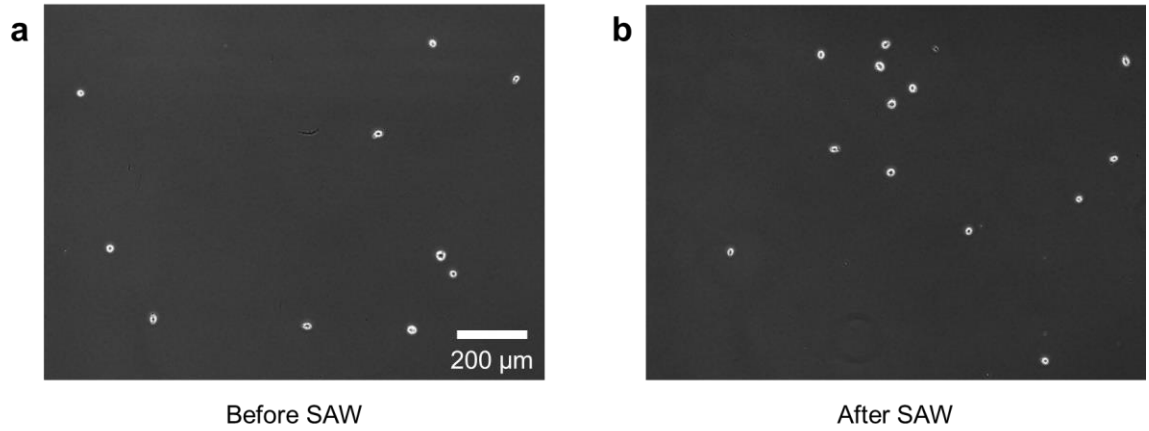

Figure S6. Cell staining for the evaluation of membrane anomalies. Cells were stained after SAW at 178.91 MHz for 10 min under room temperature (20 ℃).

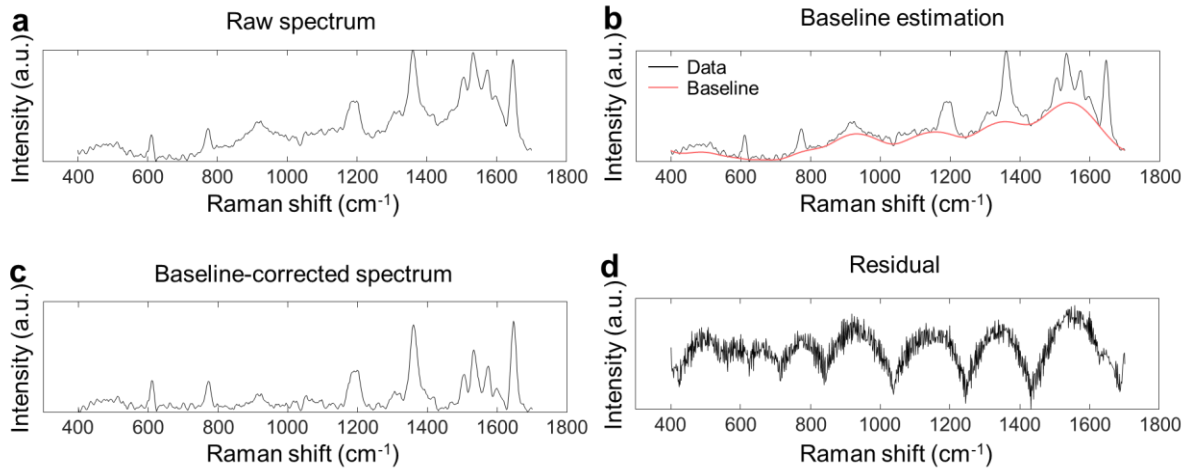

Figure S7. Baseline-correction process of raw spectrum.

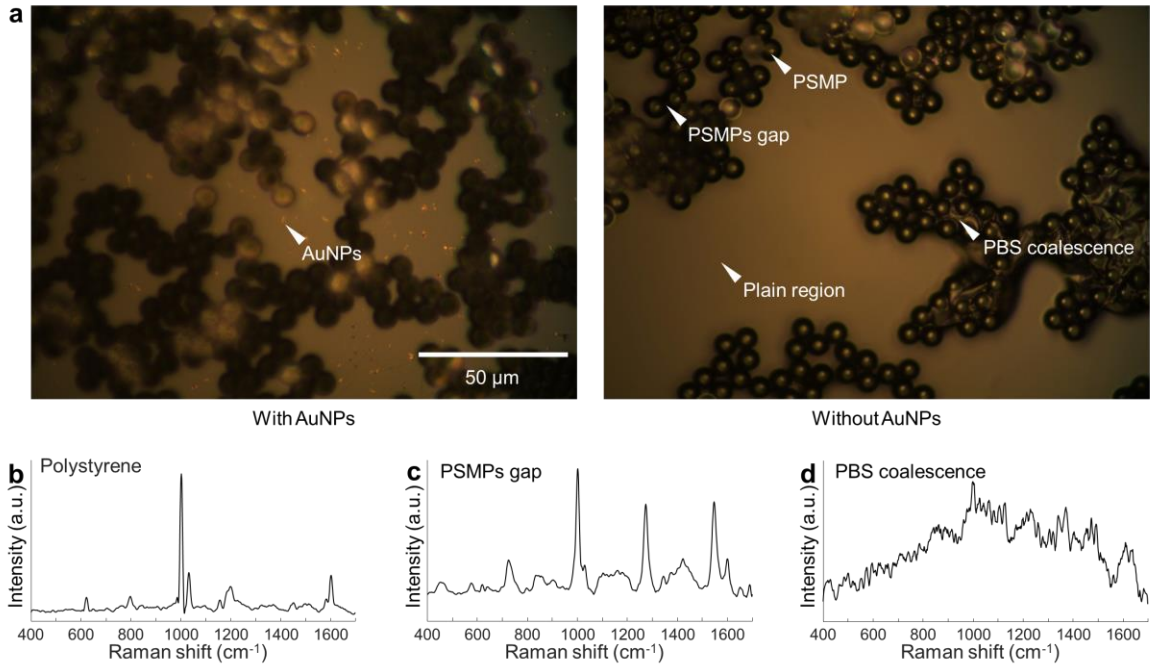

Figure S8. Spectra from different regions. a) five regions were selected to compare the signal enhancement by AuNPs. b) Raman spectrum from PSMP. c) Raman spectrum from PSMPs gap. d) Raman spectrum from PBS coalescence.

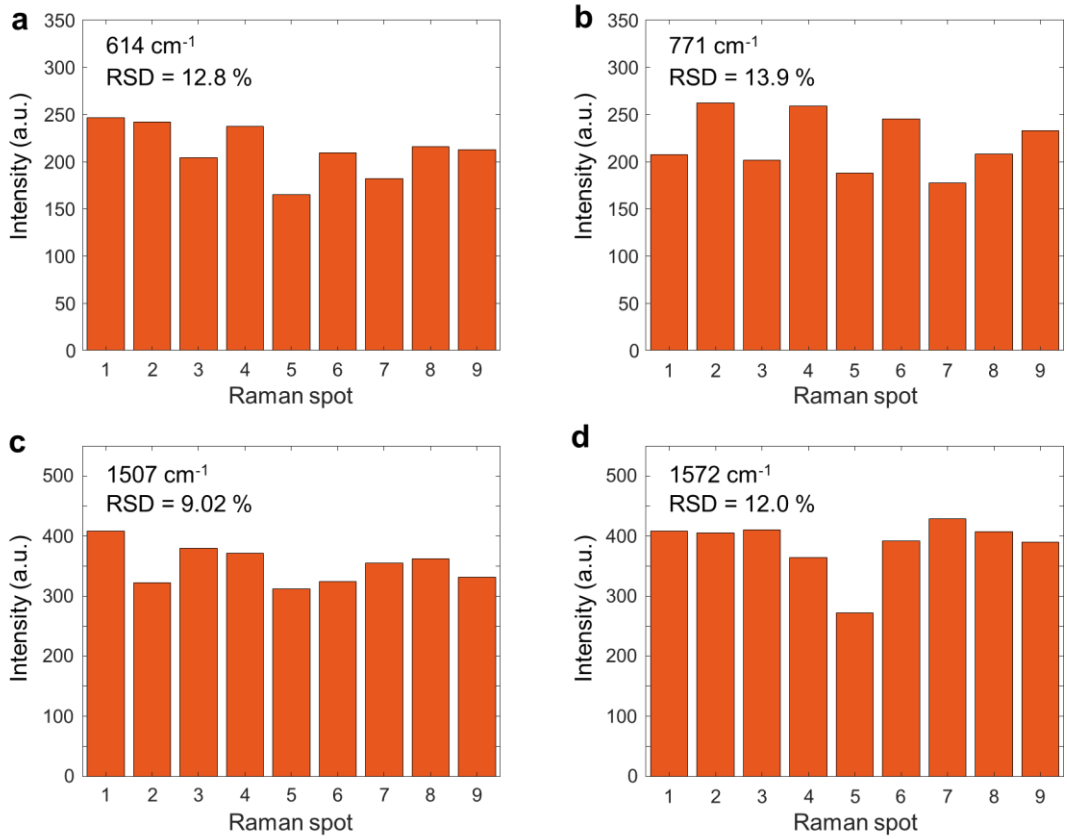

Figure S9. Relative standard deviation (RSD) values of specific peaks in R6G spectra.

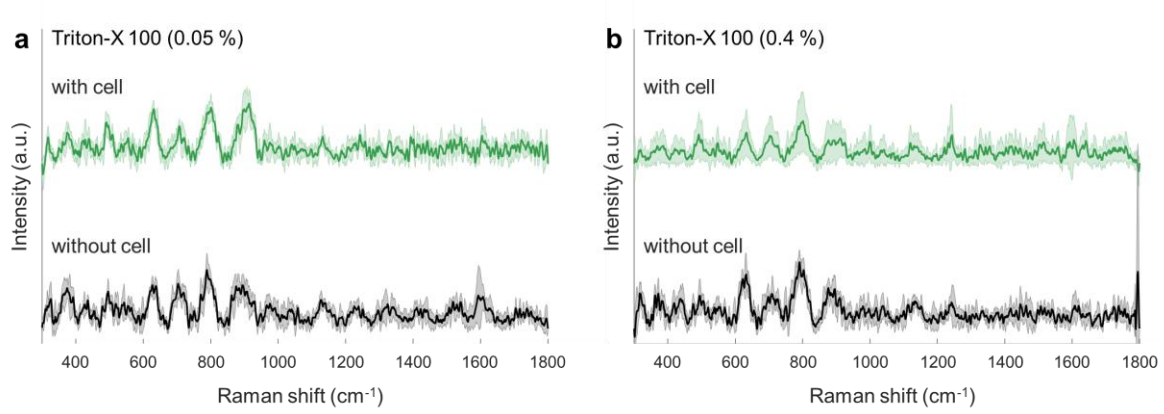

Figure S10. Mean spectra of detergent-based cell lysis. Regardless of the concentration of Triton-X 100, high noise in the spectra disturbs spectrum profiling.

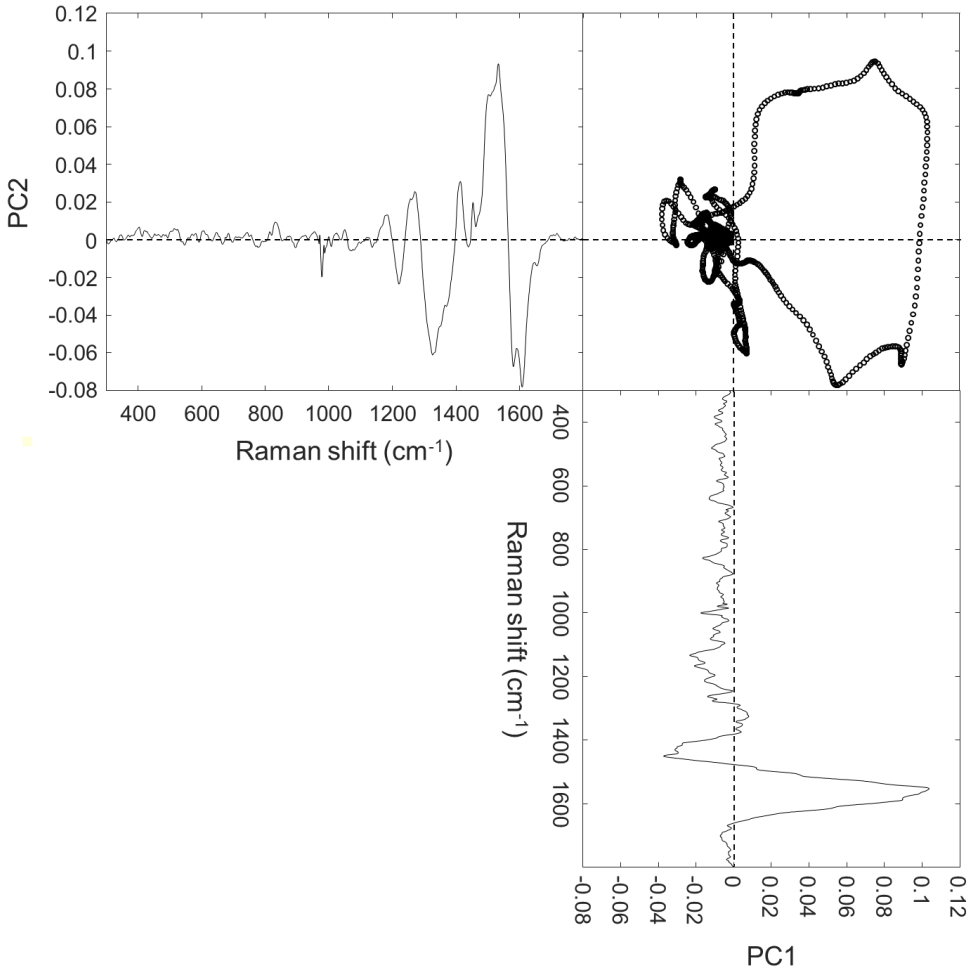

Figure S11. Loading plots for PC1 and PC2.

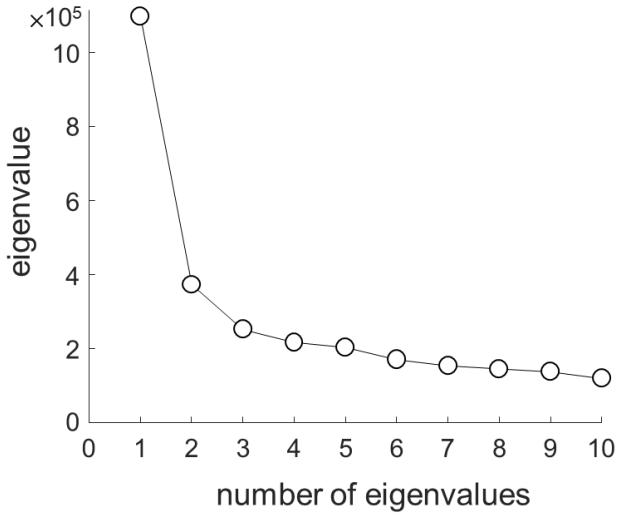

Figure S12. Scree plot for ten principal components.

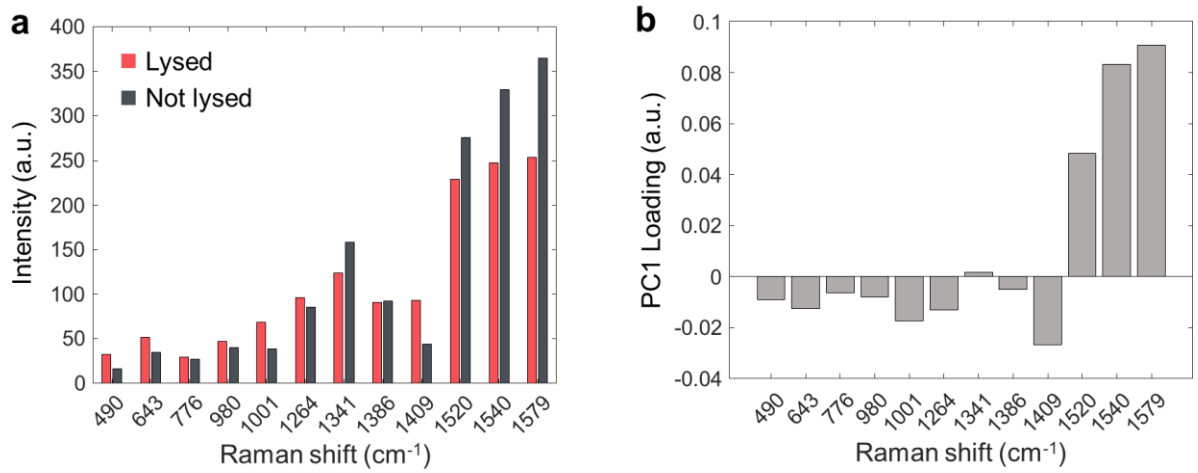

Figure S13. Comparison of specific peaks in each condition. a) Spectral intensity comparison of each condition. b) PC1 loadings of specific peaks.

Raman shift (cm^{-1})	Presumed element	References
490	Glycogen	1-3
643	C–C twisting mode of tyrosine	3, 4
776	Phosphatidylinositol	1, 5
980	C–C stretching β-sheet	1, 6
1001	Symmetric ring breathing mode of phenylalanine	3, 4
1264	=C–H in plane bending (lipid)	3, 4
1341	A and G of DNA/RNA and CH deformation of proteins	7
1386	CH_3 bend	3, 4
1409	ν_s COO^-	1, 8
1520	–C=C– carotenoids	3, 4, 9
1540	Amide carbonyl group vibrations and aromatic hydrogens	1
1579	Pyrimidine ring (nucleic acids) and heme protein	3, 4

Supplementary Table 1. Potential candidates for specific wavenumbers.

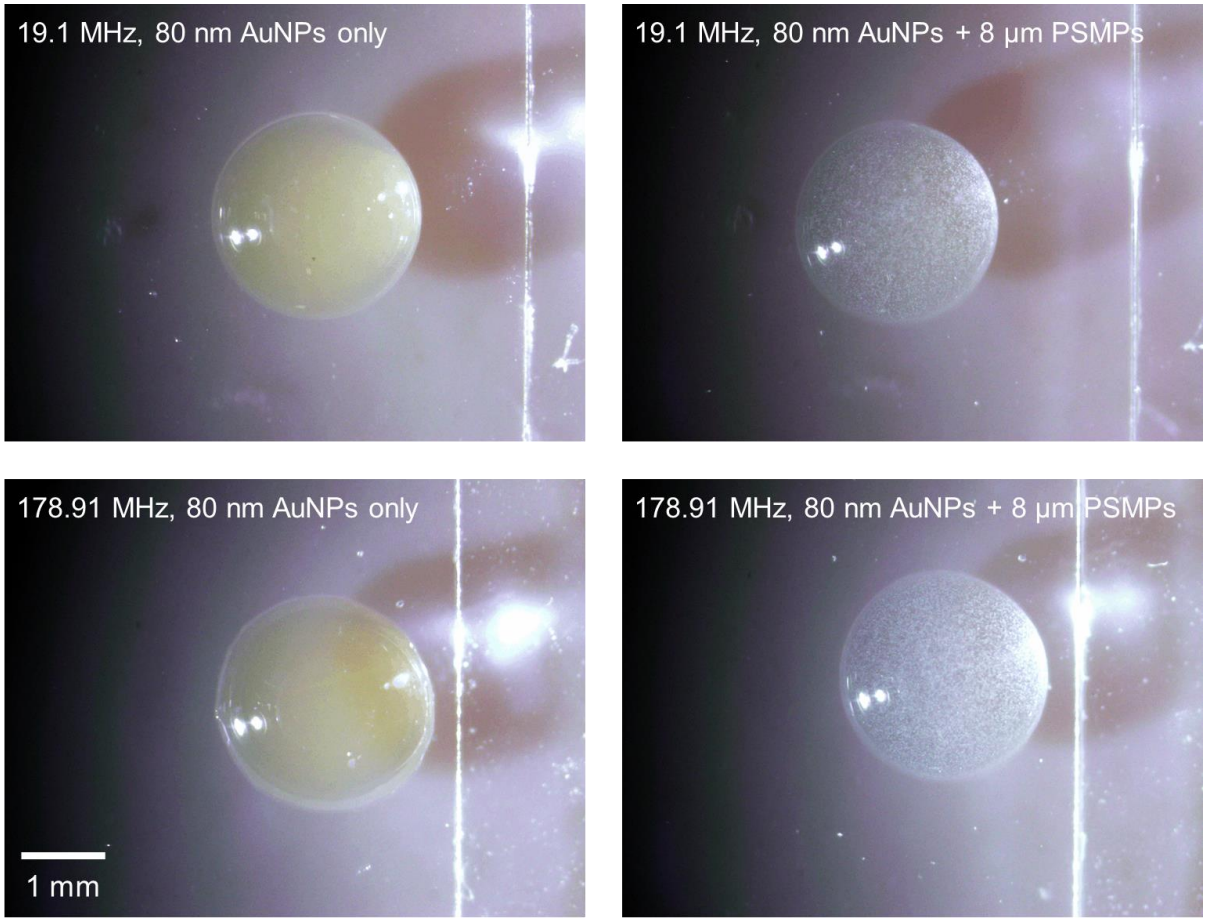

Supplementary Movie 1. Visualization of PSMPs and AuNPs. Frequency and attenuation length-dependent behaviors of PSMPs and frequency and attenuation length-independent behaviors of AuNPs.

References

1. Talari, A. C. S.; Movasaghi, Z.; Rehman, S.; Rehman, I. U., Raman spectroscopy of biological tissues. *Applied Spectroscopy Reviews* **2015,** *50* (1), 46-111.
2. Stone, N.; Kendall, C.; Shepherd, N.; Crow, P.; Barr, H., Near-infrared Raman spectroscopy for the classification of epithelial pre-cancers and cancers. *Journal of Raman spectroscopy* **2002,** *33* (7), 564-573.
3. Stone, N.; Kendall, C.; Smith, J.; Crow, P.; Barr, H., Raman spectroscopy for identification of epithelial cancers. *Faraday discussions* **2004,** *126*, 141-157.
4. Lazaro-Pacheco, D.; Shaaban, A. M.; Rehman, S.; Rehman, I., Raman spectroscopy of breast cancer. *Applied Spectroscopy Reviews* **2020,** *55* (6), 439-475.
5. Krafft, C.; Neudert, L.; Simat, T.; Salzer, R., Near infrared Raman spectra of human brain lipids. *Spectrochimica Acta Part A: Molecular and Biomolecular Spectroscopy* **2005,** *61* (7), 1529-1535.
6. Liu, Z.; Davis, C.; Cai, W.; He, L.; Chen, X.; Dai, H., Circulation and long-term fate of functionalized, biocompatible single-walled carbon nanotubes in mice probed by Raman spectroscopy. *Proceedings of the National Academy of Sciences* **2008,** *105* (5), 1410-1415.
7. Su, L.; Sun, Y.; Chen, Y.; Chen, P.; Shen, A.; Wang, X.; Jia, J.; Zhao, Y.; Zhou, X.; Hu, J., Raman spectral properties of squamous cell carcinoma of oral tissues and cells. *Laser Physics* **2012,** *22* (1), 311-316.
8. Lakshmi, R. J.; Kartha, V.; Murali Krishna, C.; R. Solomon, J.; Ullas, G.; Uma Devi, P., Tissue Raman spectroscopy for the study of radiation damage: brain irradiation of mice. *Radiation research* **2002,** *157* (2), 175-182.
9. Surmacki, J.; Musial, J.; Kordek, R.; Abramczyk, H., Raman imaging at biological interfaces: applications in breast cancer diagnosis. *Molecular cancer* **2013,** *12* (1), 1-12.